



Waves and Magnetism in the Solar Atmosphere (WAMIS)

Yuan-Kuen Ko^{1*}, John D. Moses², John M. Laming¹, Leonard Strachan¹, Samuel Tun Beltran¹, Steven Tomczyk³, Sarah E. Gibson³, Frédéric Auchère⁴, Roberto Casini³, Silvano Fineschi⁵, Michael Knoelker³, Clarence Korendyke¹, Scott W. McIntosh³, Marco Romoli⁶, Jan Rybak⁷, Dennis G. Socker¹, Angelos Vourlidas⁸ and Qian Wu³

¹ Space Science Division, Naval Research Laboratory, Washington, DC, USA, ² Heliophysics Division, Science Mission Directorate, NASA, Washington, DC, USA, ³ High Altitude Observatory, Boulder, CO, USA, ⁴ Institut d'Astrophysique Spatiale, CNRS Université Paris-Sud, Orsay, France, ⁵ INAF - National Institute for Astrophysics, Astrophysical Observatory of Torino, Pino Torinese, Italy, ⁶ Department of Physics and Astronomy, University of Florence, Florence, Italy, ⁷ Astronomical Institute, Slovak Academy of Sciences, Tatranska Lomnica, Slovakia, ⁸ Applied Physics Laboratory, Johns Hopkins University, Laurel, MD, USA

OPEN ACCESS

Edited by:

Mario J. P. F. G. Monteiro,
Institute of Astrophysics and Space
Sciences, Portugal

Reviewed by:

Gordon James Duncan Petrie,
National Solar Observatory, USA
Robertus Erdelyi,
University of Sheffield, UK
João José Graça Lima,
Institute of Astrophysics and Space
Sciences, Portugal

*Correspondence:

Yuan-Kuen Ko
yuan-kuen.ko@nrl.navy.mil

Specialty section:

This article was submitted to
Stellar and Solar Physics,
a section of the journal
Frontiers in Astronomy and Space
Sciences

Received: 02 November 2015

Accepted: 14 January 2016

Published: 16 February 2016

Citation:

Ko Y-K, Moses JD, Laming JM, Strachan L, Tun Beltran S, Tomczyk S, Gibson SE, Auchère F, Casini R, Fineschi S, Knoelker M, Korendyke C, McIntosh SW, Romoli M, Rybak J, Socker DG, Vourlidas A and Wu Q (2016) Waves and Magnetism in the Solar Atmosphere (WAMIS). *Front. Astron. Space Sci.* 3:1. doi: 10.3389/fspas.2016.00001

Comprehensive measurements of magnetic fields in the solar corona have a long history as an important scientific goal. Besides being crucial to understanding coronal structures and the Sun's generation of space weather, direct measurements of their strength and direction are also crucial steps in understanding observed wave motions. In this regard, the remote sensing instrumentation used to make coronal magnetic field measurements is well suited to measuring the Doppler signature of waves in the solar structures. In this paper, we describe the design and scientific values of the Waves and Magnetism in the Solar Atmosphere (WAMIS) investigation. WAMIS, taking advantage of greatly improved infrared filters and detectors, forward models, advanced diagnostic tools and inversion codes, is a long-duration high-altitude balloon payload designed to obtain a breakthrough in the measurement of coronal magnetic fields and in advancing the understanding of the interaction of these fields with space plasmas. It consists of a 20 cm aperture coronagraph with a visible-IR spectro-polarimeter focal plane assembly. The balloon altitude would provide minimum sky background and atmospheric scattering at the wavelengths in which these observations are made. It would also enable continuous measurements of the strength and direction of coronal magnetic fields without interruptions from the day-night cycle and weather. These measurements will be made over a large field-of-view allowing one to distinguish the magnetic signatures of different coronal structures, and at the spatial and temporal resolutions required to address outstanding problems in coronal physics. Additionally, WAMIS could obtain near simultaneous observations of the electron scattered K-corona for context and to obtain the electron density. These comprehensive observations are not provided by any current single ground-based or space observatory. The fundamental advancements achieved by the near-space observations of WAMIS on coronal field would point the way for future ground based and orbital instrumentation.

Keywords: corona, magnetic field, MHD waves, spectroscopy, polarization

INTRODUCTION

Since the advent of the Solar and Heliospheric Observatory (SOHO; Domingo et al., 1995) followed by the Transition Region and Coronal Explorer (TRACE; Handy et al., 1999; Schrijver et al., 1999) and the Solar Dynamics Observatory (SDO; Pesnell et al., 2012), the solar atmosphere has come to be increasingly appreciated as a dynamic and complex environment. The concept of a static quiescent atmosphere and corona has given way to an environment where waves play a much larger role in shaping the plasma properties than hitherto assumed, and can have non-negligible energy densities compared to the thermal gas in the low β corona. Periodic oscillations in the solar atmosphere have long been observed (e.g., Chapman et al., 1972; Roberts et al., 1983; Antonucci et al., 1984; Aschwanden, 1987; Harrison, 1987), and various oscillation modes of coronal loops have been identified (e.g., Aschwanden et al., 1999; Nakariakov et al., 1999; Wang et al., 2009). Compressive waves connected to slow mode or fast mode waves, or their analogs in inhomogeneous media, have been readily detected, but the non-compressive Alfvén wave has proven more elusive. Early claims of Alfvén wave detections (Cirtain et al., 2007; De Pontieu et al., 2007; Tomczyk et al., 2007) have been discussed (Erdélyi and Fedun, 2007; Van Doorselaere et al., 2008), and as this last reference emphasizes, the realization that Alfvén or fast mode waves (loosely collectively referred to as “Alfvénic” when close to parallel propagation where magnetic tension is the dominant restoring force) are ubiquitous in the solar upper atmosphere (McIntosh et al., 2011) signifies an important new development with profound consequences for our understanding of the corona and solar wind. More recently Jess et al. (2009) have detected Alfvén waves lower in the solar atmosphere.

Comprehensive measurements of magnetic fields in the solar corona have a longer history as an important scientific goal (e.g., Dulk and McLean, 1978; House et al., 1982; Arnaud and Newkirk, 1987; Lin et al., 2004; Tomczyk et al., 2007). As well as being crucial to understanding coronal structures and the Sun’s generation of space weather which can affect communications, GPS systems, space flight, and power transmission (Hanslmeier, 2003; Lambour et al., 2003; Iucci et al., 2006), the measurement of its strength and direction is also a crucial step in understanding observed wave motions. Most forms of solar activity, including high energy electromagnetic radiation, solar energetic particles, flares, and coronal mass ejections (CMEs), derive their energy from magnetic fields. The corona is also the most plausible source of the solar wind with its embedded magnetic field that engulfs the Earth. The ability to measure coronal magnetic fields will lead to improved predictions of hazardous space weather effects on Earth because of further understanding of the underlying physical processes.

Magnetic fields in the corona have been extremely difficult to measure for three important reasons: (1) the magnetic fields in the corona are intrinsically weak compared to the rest of the sun; (2) coronal spectroscopic lines are dimmer than their photospheric counterparts; and (3) the optically thin corona requires interpretation of magnetic signatures integrated along extended path lengths. Most knowledge to date has been derived

from extrapolations from photospheric magnetograms (see e.g., the review by Wiegmann and Sakurai, 2012; Régnier, 2013). Recently, the HAO-NCAR Coronal Multi-channel Polarimeter (CoMP) instrument (Tomczyk et al., 2008) made breakthrough measurements of the coronal magnetic field that lead to discoveries of coronal Alfvén waves (Tomczyk et al., 2007), as well as advancement in the magnetic structure in prominences and coronal cavities (Dove et al., 2011; Bak-Stešlicka et al., 2013). However, such ground observations are still limited by the sky background, atmospheric seeing effect and the day–night and weather related interruptions. With such observations from space still lacking and the prospect of such instrumentation on a space mission still uncertain, the most sensible way is to take the measurements from above the atmosphere with long-duration balloon flights.

In this paper, we describe the design and scientific values of the Waves and Magnetism in the Solar Atmosphere (WAMIS) investigation. In *The Importance of Magnetic Field and Waves Measurements in the Corona* we describe the importance of coronal magnetic field and waves measurements in answering current outstanding questions in solar physics. WAMIS Instrument Concept describes the observational requirements, methodology and the WAMIS Instrument Design for making breakthroughs in the coronal field measurements. Concluding remarks gives some concluding remarks.

THE IMPORTANCE OF MAGNETIC FIELD AND WAVES MEASUREMENTS IN THE CORONA

In this section, we describe major outstanding questions in solar physics research that illustrate the importance of direct measurements of the coronal magnetic field in its strength, structure and dynamics.

What Determines the Magnetic Structure of the Corona?

The large-scale coronal structure is a consequence of surface field advection, differential rotation, and photospheric flux emergence. Information on the evolution and interactions between magnetically closed and open regions could shed light into understanding the changing structure of the heliospheric magnetic field and how the slow solar wind is formed. The fast solar wind has been known for some time to originate in open field regions, i.e., coronal holes (e.g., Krieger et al., 1973). The origins of the slow wind are more obscure, but are thought to be at the interface between open and closed field where reconnection opens up previously closed regions (e.g., Fisk and Schwadron, 2001). This idea has been refined recently by Antiochos et al. (2011) in terms of the S-web (“S” stands for separatrix), where extensions from the polar coronal holes reach down to lower latitudes, allowing open field and closed field regions to interact.

Coronal magnetic field measurements would allow a reconstruction of magnetic field in the extended corona from which the topology of the S-web could be estimated. Also, turbulence in the slow wind is known to be more “balanced”

than in the fast wind (e.g., Bruno and Carbone, 2005), meaning that the amplitudes of waves propagating in opposite directions along the magnetic field are more nearly equal than in the fast wind. The existing claims for coronal Alfvén wave detections (Cirtain et al., 2007; De Pontieu et al., 2007; Tomczyk et al., 2007; Tomczyk and McIntosh, 2009; Okamoto and De Pontieu, 2011) often see a preponderance of waves propagating in one direction (i.e., upwards), more consistent with fast wind. More recently De Moortel et al. (2014) and Liu et al. (2014) have seen upward propagating waves at both loop footpoints meeting at the apex and generating higher frequency (presumably balanced) turbulence. In the likely case that this difference in turbulence has its origin in the solar wind source regions, measurement of waves in the corona has unique potential to distinguish between slow and fast wind in this way, and thus investigate their interface. Such investigations are ideally suited to solar minimum conditions when polar coronal holes are better defined and magnetic topology is less complex than at solar maximum.

Another distinction between fast and slow solar wind lies in their elemental compositions. The fast wind is relatively un-fractionated, while the slow wind exhibits an enhancement in abundance of elements with first ionization potential (FIP) less than about 10 eV (the so-called “FIP Effect”; e.g., see von Steiger et al., 1995; Feldman and Laming, 2000). This effect is most convincingly explained in terms of the ponderomotive force in the chromosphere, resulting from the propagation through or reflection from the chromosphere of Alfvén waves (Laming, 2004, 2009, 2012, 2015; Rakowski and Laming, 2012) with peak amplitudes in the corona of $25\text{--}100\text{ km s}^{-1}$, depending on the chromospheric model and coronal density. This amplitude is larger than that typically associated with nonthermal mass motions inferred from spectral line broadening by a factor of up to 4, but evidence for such motions has more recently been documented (e.g., Peter, 2001, 2010). CoMP sees much lower Doppler velocity amplitudes than these (Tomczyk et al., 2007), but McIntosh and De Pontieu (2012) argue that this is due to line of sight (LoS) superposition effects “hiding” the true coronal wave flux in enhanced non-thermal broadening. FIP fractionated closed loops should show more balanced waves than less fractionated open field regions, due to repeated Alfvén wave reflection from the chromosphere, consistent with presumed origin of the slow wind in a fractionated closed loop and the fast wind in a relatively un-fractionated open field region. De Moortel et al. (2014) and Liu et al. (2014) see something like this in CoMP observations of coronal loops, though the balanced turbulence is restricted to the apex region, and is observed at higher frequencies possibly indicating an onset of turbulent cascade where upcoming waves from each footpoint meet. The interpretation of decreasing spectral line widths with height above a coronal hole in terms of Alfvén wave damping (Hahn et al., 2012; Hahn and Savin, 2013) would lead to the prediction of a similar phenomenon in open fields, if the Alfvén wave damping proceeds by turbulent cascade. Counter propagating Alfvén waves have recently been detected in coronal holes (Morton et al., 2015), supporting this inference. Further, Alfvén and fast mode waves also behave differently around coronal null points, also represented by separatrices or quasi-separatrix layers. Fast

mode waves refract across field lines and accumulate at the null point, leading to increased wave heating, while Alfvén waves are confined to magnetic field lines (Thurgood and McLaughlin, 2013). Detecting these waves directly would provide valuable information for distinguishing the solar wind formation and acceleration mechanisms in both the fast and slow solar wind.

How are Flux Ropes Formed, How Do they Evolve, and How are they Related to CMEs?

Opposing views exist regarding the nature of flux tubes in active regions. Some authors suggest that coronal loop must have twisted field, in order to give it a distinct identity, separate from other coronal magnetic field (e.g., Hood et al., 2009; Vasheghani Farahani et al., 2010), and to be sufficiently buoyant to emerge from the convection zone (e.g., Archontis, 2008). Others argue that newly emerged flux is untwisted, and the flux rope signatures seen in *in situ* observations of ICMEs arise due to reconnection of a sheared arcade during the CME eruption (e.g., Lynch et al., 2004) or a pre-CME flare (Patsourakos et al., 2013). Sakai et al. (2001) found that torsional waves in twisted high β (≈ 1) loops propagate preferentially in a direction that unwinds the twist. Observations of constant cross sectional loops have been interpreted as being due to circular loops necessarily exhibiting significant twist (Klimchuk, 2000). More recent studies suggest that this is an observational selection effect, and that coronal magnetic field is asymmetric and untwisted (Malanushenko and Schrijver, 2013). The distinction is important, relating to the mechanisms by which flux emerges, CMEs erupt, and the nature of waves on such structures. Pure torsional Alfvén waves may only propagate on untwisted flux tubes (Vasheghani Farahani et al., 2010). The twist necessarily introduces mixing between Alfvén and kink modes, with consequences for the wave damping and coronal heating. The absence of intensity oscillations seen by CoMP (Tomczyk et al., 2007) suggests that any torsional waves in the solar corona must have been propagating on untwisted magnetic field.

Observing the magnetic structure of various loops, including prominences, and prominence flows, e.g., through He I 1083.0 nm, together with observations of the chromospheric magnetic fields under the same structure, once inverted (e.g., Orozco Suárez et al., 2014), could place constraints on prominence densities and determine how prominence and coronal magnetic fields interact, how and where magnetic energy is stored (e.g., flux and helicity transport) and how it is released (e.g., instabilities, reconnection, dissipative heating). In particular, measurements of prominence cavities obtained by the CoMP instrument indicate a characteristic “lagomorphic” signal (i.e., morphologically shaped like a rabbit’s ear) in linear polarization consistent with twisted magnetic flux tubes, or ropes. Bak-Stešlická et al. (2013) showed that coronal prominence cavities, for example as observed by SDO/AIA193Å channel, are observed by CoMP to have such linear polarization signature in the Fe XIII 1074.7 nm line. This signature can be explained as arising from an arched magnetic flux rope with axis oriented along the LoS (e.g., Fan, 2010; Gibson et al., 2010). When

integrated along the LoS, a combination of linear polarization nulls occurring where the flux rope magnetic field is oriented at the van Vleck angle θ , ($\cos^2\theta = 1/3$), or where the axial magnetic field is oriented completely out of the plane of sky (PoS), leads to a forward-modeled signal of the same characteristic shape as observed. Linear polarization is sensitive to PoS magnetic field, so a “polarization ring” may occur when magnetic field winds around a central LoS-oriented axis. Indeed, early CoMP observations of a prominence cavity showed just such a structure (Dove et al., 2011). LoS effects play an important role so that such a pure ring may be rare, and may also indicate a different magnetic topology to the flux ropes in Bak-Steslicka et al. (2013). However, analysis of CoMP observations indicate a truly ubiquitous lagomorphic structure in linear polarization observed in Fe XIII associated with prominence cavities that matches expectations for the linear polarization signal of a forward-modeled, arched magnetic flux rope fully integrated along the LoS (e.g., Rachmeler et al., 2013). Analysis of the circular polarization of such structures would confirm the presence of a magnetic axis and quantify its field strength. Inside prominences, similar studies may be undertaken with the He I 1083.0 nm line, while outside a coronal line, such as Fe XIII 1074.7 nm, can be used.

Where Do CME-Associated Shocks Form?

Particles accelerated by CME-driven shocks have the highest particle energies of all suprathermal species and pose the greatest space weather hazards to spaceborne instrumentation and humans. The very highest SEP energies arise when acceleration begins very close to the sun. Gopalswamy et al. (2001) and Mann et al. (2003) use model magnetic fields and density profiles for different solar regions, with particular attention to active regions, to estimate the heliocentric radius where a CME driven disturbance becomes a shock (i.e., Alfvén Mach number, $M_A > 1$), and where it becomes supercritical ($M_A > 2-3$, depending on plasma β and shock obliquity). This last transition is crucial, because it determines where the shock begins to become turbulent and may begin to reflect and accelerate particles (Edmiston and Kennel, 1984), in the absence of pre-existing seed particles.

Measurements of the electron density and constraints on the magnetic field within about $1.25 R_\odot$ (where the Fe XIII 1074.7 nm/1079.8 nm line pair is sensitive to electron density) would remove the ambiguities introduced in the model for these quantities entering in the calculation of the Alfvén speed. Further the magnetic field PoS direction allows inference of the CME shock obliquity. Such shocks are currently believed to propagate close to the Sun as quasi-perpendicular, evolving to quasi-parallel further out (Tylka and Lee, 2006; Rouillard et al., 2011). This has consequences for particle acceleration (Laming et al., 2013). More sophisticated current shock acceleration theories generally treat only the parallel case (e.g., Ng and Reames, 2008).

Coronal magnetic field measurements during the passage of a CME can detect compressions and distortions in the magnetic field as well as associated waves due to the formation and passage of a CME shock. Density compressions resulting from shock formation can be large enough to produce intensity enhancements in white light coronal images as well

(Vourlidas et al., 2003) that are complementary to coronal field measurement for understanding the CME shock and its role in producing SEPs.

How is Energy Stored and Released by Reconnection in Coronal Heating, Flares and CMEs?

Most observations designed to detect signatures of magnetic reconnection in the solar corona to date have focused on observing high temperature plasma, specifically high electron temperatures. While observations of CME current sheets have been successful in this respect (e.g., Ciaravella et al., 2002; Ko et al., 2003; Ciaravella and Raymond, 2008; Savage et al., 2010), searches of the solar corona for evidence of nanoflare heating have been less clear (e.g., Brooks et al., 2009). Observations by Hi-C (Cirtain et al., 2013) suggest that both nanoflares (e.g., Testa et al., 2013) and steady heating (e.g., Warren et al., 2010; Peter et al., 2013), presumably associated with waves, are present. Such waves are often suggested to propagate up from the convection zone (e.g., Asgari-Targhi et al., 2013), although reconnection is also a potential source of waves (e.g., Sturrock, 1999; Longcope et al., 2009; Kigure et al., 2010; Liu et al., 2011), and offers another interpretation of the results of De Moortel et al. (2014). Hence it appears that the detection and identification of different modes of magneto-hydrodynamic (MHD) waves, combined with observations of magnetic topology, would be highly constraining on the nature and existence of magnetic reconnection at the heart of an active region. The magnetic free energy could be calculated from the non-potential field (e.g., extrapolated from photospheric or chromospheric magnetograms), and compared with energetics of the active region.

Direct experimental knowledge of LoS magnetic field strengths before and after a CME eruption would allow estimation of the magnetic energy released, for comparison with measurements of CME kinetic, thermal and gravitational energy. This would be complementary to the estimates derived from field extrapolations. It would also allow an assessment of the likely mechanism of CME eruption (see e.g., Ugarte-Urra et al., 2007) from the change in magnetic topology. The LoS field strength and PoS direction together provide diagnostics for magnetic topologies, including magnetic nulls and current sheets that can be compared to the location of high temperature emission.

WAMIS INSTRUMENT CONCEPT

The Waves and Magnetism in the Solar Atmosphere (WAMIS) investigation is a long duration balloon (LDB) based 20 cm aperture coronagraph designed to meet challenges of answering these outstanding questions. WAMIS builds on the heritage of CoMP (Tomczyk et al., 2008), and could obtain continuous measurements over at least 2 weeks of the strength and direction of coronal magnetic fields within a large field-of-view (FOV) at the spatial and temporal resolutions required to address outstanding problems in coronal physics. The key WAMIS characteristics are summarized in **Table 1**. Additionally, the WAMIS investigation would make near simultaneous

TABLE 1 | WAMIS long duration balloon instrument characteristics.

Telescope type	Internally occulted Lyot coronagraph
Objective lens	f/10 singlet, aperture 20 cm, focal length 203.3 cm
Objective Stray Light	<0.2 μ B _⊙ goal, 1.2–2.8 R _⊙ (B _⊙ = 9.34 × 10 ⁶ erg/cm ² /s/sr/nm)
Overall Throughput	≈5%
Plate Scale	4.5"/pixel low magnification mode; 1.5"/pixel high magnification mode
Fe XIII (1074.7 nm) Count Rate @ 1.1 R _⊙	1 × 10 ⁵ photons/pixel/s @ 1.5"/pixel magnification
Detector	Goodrich Visible+SWIR camera, 15 micron pixels, 1280 × 1024 format
Inner FOV Limit	1.02 R _⊙
Outer FOV	±2.8 R _⊙ @ 4.5"/pixel Sun Centered; 1.8 R _⊙ @ 1.5"/pixel Limb Centered
Primary Lines of Interest	Fe XIII (1074.7, 1079.8 nm); AR observations; Fe X (637.5 nm), Fe XI (789.2 nm); CH&CHB observations; He I (1083.0 nm); prominence/flux rope observations
Filter	Tunable Lyot filter, 3.8 cm aperture, 530–1100 nm range
Duration of Continuous Observational Sequence	2 weeks minimum; ≥4 weeks optimum

observations of the electron scattered K-corona for context and to establish electron density out to greater radial distances than those accessible with the Fe XIII 1074.7 nm/1079.8 nm intensity ratio (~1.25 R_⊙; wavelengths given here and elsewhere are values in air). These comprehensive observations are not provided by any current single observatory. The visible-IR spectral range covers emission lines for understanding the magnetic field strength and structure in the active region (AR) and coronal hole (CH), the coronal hole boundary (CHB) region relevant for solar wind studies, as well as the prominence/flux rope structures. Observations of MHD waves would address fundamental issues in coronal heating and the sources and acceleration of the solar wind. In particular, the cross helicity of observed waves (from Fe XIII together with Fe X 637.5 or Fe XI 789.2 nm) should allow an empirical distinction between “balanced” turbulence in the slow wind, compared to more directed turbulence in the fast wind (e.g., Bruno and Carbone, 2005). Since coronal waves detected so far are ubiquitously “Alfvénic,” their direction of propagation indicates the magnetic field vector [either because of their natural properties (Alfvén mode), or because of refraction to high density that follows the magnetic field (fast mode)], and such observations obviously complement direct magnetic field measurements.

Observational Requirements

The science questions in Section The Importance of Magnetic Field and Waves Measurements in the Corona could be addressed through observation of coronal magnetic fields and waves over a 1.02–1.8 R_⊙ FOV with high spatial resolution of 1.5" or an alternative 1.02–2.8 R_⊙ large-FOV mode with a spatial resolution of 4.5", at a temporal cadence of 5 min (see Section Advantages of Measurements Outside of the Atmosphere for more detail). At this cadence, WAMIS would be sensitive to magnetic field

strengths of <10 Gauss for the faintest detectable coronal structures and one Gauss for the brightest. A spatial resolution of 4.5" is sufficient to address many of the scientific questions pertaining to the global magnetic structure of the corona, while the 1.5" resolution allows a more detailed view of individual coronal features. The capability for the higher spatial resolution observations (1.5") over a more limited FOV would be achieved with interchangeable magnification lenses. This new capability of WAMIS is potentially important for observations of active region loops, and represents a significant improvement on the capabilities of CoMP. According to McIntosh and De Pontieu (2012), WAMIS should see correspondingly higher Alfvén wave amplitudes than CoMP, due to reduced confusion caused by spatial-averaging. The large FOV of WAMIS (up to 2.8 R_⊙ from Sun center) would be needed to observe the global properties of the corona and is required to address the science questions, concerned with tracking the outward motion and other basic properties of the solar wind, CMEs and prominences as they are ejected from the corona. It is also necessary to observe as low in the corona as possible to understand how the corona continually reacts to changes occurring in the photosphere and chromosphere. High temporal cadence is needed to capture the relentless dynamic evolution of the coronal plasma structure and explosive disturbances (e.g., MHD waves, shocks, prominence eruptions, CMEs). The physical properties of CMEs and eruptive prominences are best determined from the polarization signal of broadband filtered white-light observations because the scattered light from the corona is partially polarized. Furthermore, the absence of all atmospheric seeing effects (not just sky brightness) could prove to be a critical advantage to balloon-borne as opposed to ground-based instrumentation.

Note that a 5 min cadence for magnetic field measurement does not limit the minimum wave frequency WAMIS can measure, because wave observations (unpolarized) would not need the same accumulated exposure time for a given signal-to-noise ratio (S/N, see discussion of magnetic field S/N in Section Improved Sensitivity for Measurement of the Magnetic Field Strength). Depending upon the intensity of the target structure for wave observations, the image cadence could be as short as 2 s, thus detecting waves of period as low as 1 min. The images required for a wave investigation at this cadence would not necessarily require a different observational program from the magnetic field observing program. Thus the wave and magnetic field observing programs could run simultaneously, even though the cadence of the two measurements generated by post-flight analysis would be very different.

Table 2 shows the science traceability matrix. There is a specific need to directly measure the magnetic field both in the corona and in the chromosphere. Recent observations suggest that MHD waves in the upper chromosphere have sufficient energy to accelerate the solar wind outside of active regions (Aschwanden et al., 2007; De Pontieu et al., 2007; McIntosh et al., 2011), if they can escape into the corona. WAMIS would provide routine magnetic field and wave measurements in this key region and would complement observations of activity lower in the solar atmosphere such as by the Interface Region Imaging Spectrograph (IRIS, De Pontieu et al., 2014)

and Chromosphere and Prominence Magnetometer (ChroMag, de Wijn et al., 2012), already under development, and planned for deployment at Mauna Loa Solar Observatory (MLSO) by 2016. These measurements altogether would provide critical information on the magnetic and plasma conditions to couple the coronal magnetic fields with those measured at photospheric heights.

Advantages of Measurements Outside of the Atmosphere

Improved sensitivity for measurement of the magnetic field strength

In order to achieve such observational requirements, WAMIS would need to observe features down to a few millionths of the brightness of the solar disk ($2 \times 10^{-6} B_{\odot}$ or $2 \mu B_{\odot}$), which requires an effective sky background an order of magnitude lower (e.g., $0.2 \mu B_{\odot}$). For example, bright loops above active regions are typically of the order of $20\text{--}25 \mu B_{\odot}$ while in coronal holes the brightness is typically $1\text{--}2 \mu B_{\odot}$. One objective of the WAMIS instrument would be to perform coronal magnetometry using the forbidden emission lines of Fe XIII at 1074.7 and 1079.8 nm and the He I emission line at 1083.0 nm. While coronal magnetometry would not be the only objective of WAMIS, it is instructive to consider the details of this measurement from outside the atmosphere.

Because the amplitude of the Zeeman-induced circular polarization (Stokes V) signal is $\approx 10^{-3}$ for a 10 G field for

the Fe XIII 1074.7 nm line [the linear polarization signal is typically 2 orders of magnitude higher (Lin et al., 2000; Tomczyk et al., 2008)], the S/N requirement for the circular polarization measurements drives the requirement for coronal magnetometry (such as by enlarging the aperture of the coronagraph or longer integration time to obtain better counting statistics). For ground-based observations, stray light in the form of sky brightness is usually the dominant noise source. The expected noise in the LoS component of the coronal field due to the combination of photon counting statistics in the signal and in the stray light background can be derived from consideration of the propagation of errors in the circular polarization measurements (Penn et al., 2004), and is given by

$$\sigma_B[G] = \frac{8500}{\sqrt{I_{\text{line}}}} \sqrt{1 + 2 \frac{I_{\text{sky}}}{I_{\text{line}}}} \quad (1)$$

where I_{line} and I_{sky} are the number of photons in the emission line and background, respectively. This equation assumes photon noise limited observations in the Fe XIII 1074.7 nm (Landé g factor = 1.5) emission line. Note this equation ignores all other atmospheric seeing effects generating noise in the polarization measurement except for atmospheric stray light (sky brightness). Equation (1) shows that the presence of sky background (including instrument scattered light) reduces the effective aperture of the telescope. That is the reason why long integration times are needed from the ground to achieve the desired polarimetric sensitivity. From MLSO, where CoMP is located, the sky brightness is nominally $5.0 \mu B_{\odot}$. However, for balloon-borne observations, internally generated stray light of the coronagraph dominates the sky background. For the internally occulted design of WAMIS a conservative estimate of the stray light-generated sky background is equivalent to $I_{\text{sky}} = 0.2 \mu B_{\odot}$. We can combine Equation (1) with a flux budget for the corona and compute the expected noise level as a function of coronagraph aperture size and coronal brightness. This is illustrated in **Figure 1**, assuming a system throughput of 5%, a pixel of $5''$, and an integration time of 5 min. On the left are balloon-borne observations where the stray light is strictly generated by the coronagraph (e.g., $0.2 \mu B_{\odot}$). On the right are

TABLE 2 | Science traceability matrix; see text for details.

Science Objective	FoV/Spatial Resolution	Physical Observable
1. Fast/Slow Wind, Coronal B structure	1.02–1.8 $R_{\odot}/1.5''$ pix.; 1.02–2.8 $R_{\odot}/4.5''$ pix.	Waves: Doppler velocity, plasma density, B-field direction
2. Prominences, flux ropes	1.02–1.8 $R_{\odot}/1.5''$ pix	B-field magnitude & direction from He I and Fe XIII
3. CME Shocks	1.02–2.8 $R_{\odot}/4.5''$ pix.	B-field magnitude & direction, Waves: Doppler velocity, plasma density
4. Reconnection	1.02–1.8 $R_{\odot}/1.5''$ pix.	B-field magnitude & direction, Waves: Doppler velocity, plasma density

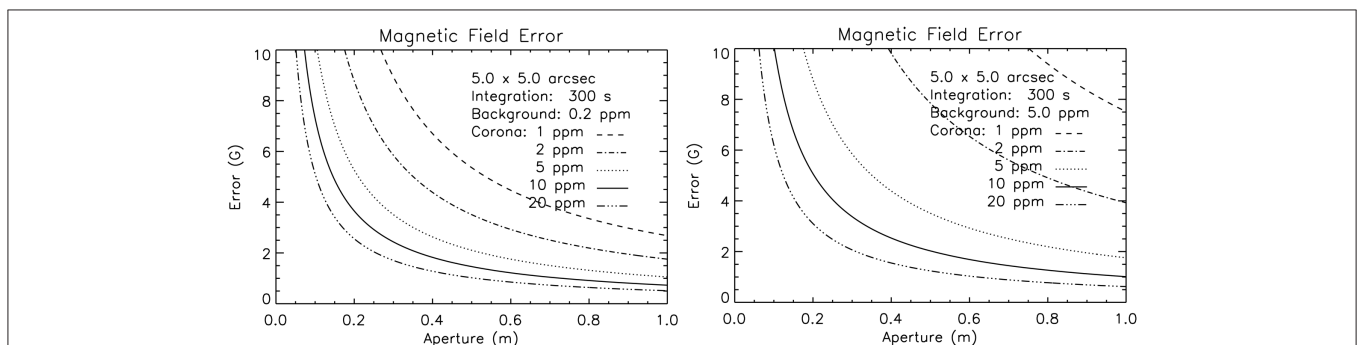


FIGURE 1 | These plots illustrate the impact of stray light on the relationship between LoS magnetic field strength sensitivity in Fe XIII 1074.7 nm and telescope aperture (see text for detail).

observations at MLSO where a typically good sky background is $5.0 \mu B_{\odot}$. The lines plotted correspond to various intensities of the corona in μB_{\odot} units. With balloon-borne observations, it is possible to achieve magnetic field sensitivities of 3.5 G in 5 min for coronal structures with brightness of $10 \mu B_{\odot}$ using a 20 cm aperture telescope. From a similar instrument from the ground (i.e., CoMP at MLSO), with 5 min integration one achieves a sensitivity of 5 G. The needed integration time to reach comparable σ_B on the ground would be two times longer.

Figure 2 compares the modeled Fe XIII 1074.7 nm Stokes V signal integrated for 1 h for the sky background expected for WAMIS vs. that for CoMP. The larger circular polarization signal of a balloon-borne WAMIS is obvious. For example, Rachmeler et al. (2013) modeled the linear and circular polarizations from a flux rope and a sheared arcade. They showed that the true disambiguator between the two magnetic models is the circular polarization. A flux rope will have a clearly defined magnetic axis, where the circular polarization (proportional to the LoS magnetic field) will peak. This demonstrates the importance and advantage of performing IR coronal magnetometry from a balloon-borne or space platform.

Eliminating seeing effect through the Earth's atmosphere

Near-space observations on a balloon platform would eliminate all polarization noise (variability) introduced by the Earth's atmosphere which is difficult to quantify for ground-based observations. This would provide a fundamental advantage in the interpretation of all coronal magnetometry observations, including observations with future larger aperture ground-based instruments, e.g., the Daniel K. Inouye Solar Telescope (DKIST), and the Coronal Solar Magnetism Observatory (COSMO). A second advantage would be to allow WAMIS

to forego simultaneous continuum observations required for ground-based instruments (such as the Wollaston prism on CoMP, Tomczyk et al., 2008). Therefore, the full imager plane can be used for the line image resulting in an increase in routine spatial resolution for a given detector format and FOV. While continuum images do not need to be obtained simultaneously with the line images, they could be obtained at appropriate intervals to provide reference background and K-corona imaging.

Enabling continuous observations

The continuity of balloon-borne observations (independent of atmospheric variation, and no day/night cycle and weather-related interruptions) could be used to integrate signals over extended periods of time and beat down the photon noise. Coronal cavities associated with polar crown prominences would be good candidates for such a study, since they tend to be dynamically stable and are extended along the LoS, so that they can be essentially unchanged for up to several days of limb observations. Since most coronal lines observed by WAMIS are optically thin plasma projected against the PoS, this advantage is critical in separating the 3-D structure of the corona from short-term evolution of the corona. Uninterrupted observations also increase the probability of detecting and following solar transient events. In addition, uninterrupted observations of over 2 weeks with the expected magnetic field sensitivity of WAMIS could in principle enable tomographic inversions for 3D magnetic field vector (Kramar et al., 2006, 2013; Judge et al., 2013).

Advantages of the Large Field-of-View

The FOV of WAMIS (1.02 – $2.8 R_{\odot}$) would enable analysis of the global magnetic topology of the corona. For example, Rachmeler

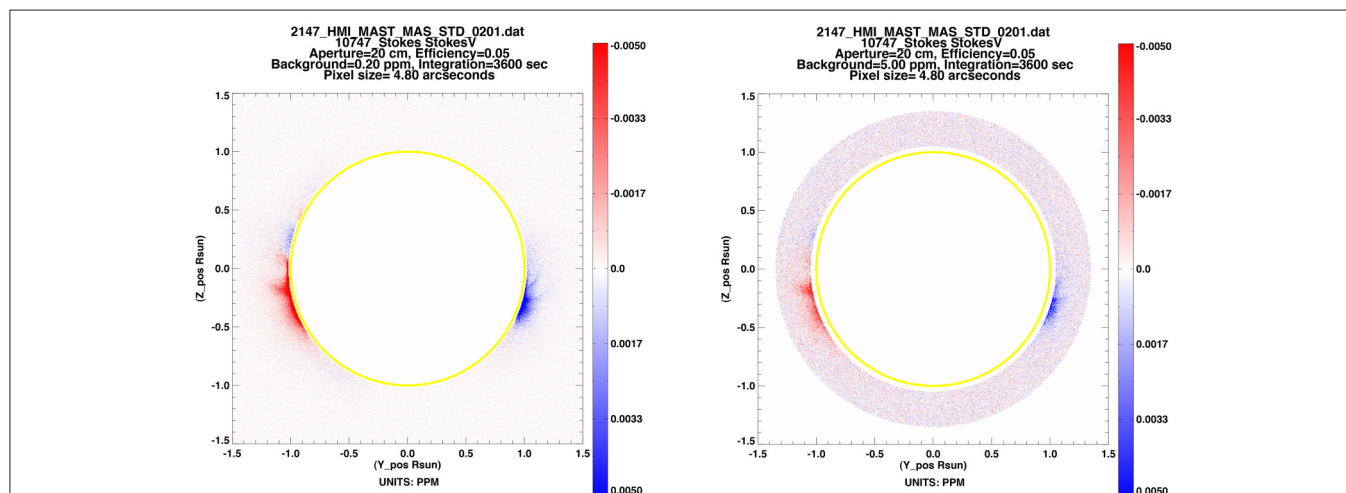


FIGURE 2 | Comparison of forward-modeled circular polarization for a global coronal MHD model (Predictive Science Inc. MAS model for Carrington Rotation 2147, from http://www.predsci.com/hmi/data_access.php), and applying the FORWARD SolarSoft codes (<http://www.hao.ucar.edu/FORWARD/>). Photon noise is added based on telescope aperture, efficiency, background, pixel size, and integration time. Left: Background = 0.2 PPM (i.e., $0.2 \mu B_{\odot}$, appropriate for WAMIS), Right: Background = 5 PPM (appropriate for CoMP), all integrated for 1 h. WAMIS vs. CoMP FOVs are explicitly applied to these images as internal/external occulters (at $1.02/1.05$, $2.8/1.35 R_{\odot}$ respectively). Note that sources of systematic errors are not considered, but are expected to be significant since the signal shown here is on the order of 0.1% of intensity.

et al. (2014) forward modeled Fe XIII signals for pseudostreamers vs. double streamers and found clear distinctions between these magnetic topologies arising from the null point lying above the pseudostreamer (at $\sim 1.4 R_{\odot}$). Analysis of PROBA2 Sun Watcher using Active Pixel System Detector and Image Processing (SWAP) data yielded structures in EUV that aligned with the expected distinctions in morphology, but the Fe XIII 1074.7 nm linear polarization topological measurement was limited by the CoMP FOV. WAMIS will be able to unambiguously reveal the pseudostreamer topology. The large FOV would also allow better tracing of the evolution of the CME dynamics from the line intensity, Doppler shift and width (Tian et al., 2013). As a comparison, the up to 5 arcmin FOV of DKIST is not designed for studies of the global coronal structure and CMEs, and the 1.05–1.35 R_{\odot} FOV of CoMP would miss a significant fraction of the null points in coronal structures and post-CME current sheet, as well as the likely formation of SEP-produced CME shocks above 1.5 R_{\odot} .

Coronal Magnetometry via Zeeman and Hanlé Effect

The Zeeman effect in forbidden coronal lines can provide information on coronal magnetic fields with strengths as low as a fraction of a Gauss and as high as several thousand Gauss. This is very important as it provides information on both the large-scale “quiet” coronal fields as well as the active region fields. The observations are restricted to off-limb observations obtained with coronagraphs (or at total solar eclipses) and in which LoS integration issues arise, because of the small optical depths in the corona. However, this is not an overwhelming issue as argued by Judge et al. (2013). To address the LoS confusion of coronagraph observations one can use coincident white-light and EUV observations such as those from the Solar Terrestrial Relations Observatory (STEREO), the Large Angle and Spectrometric Coronagraph Experiment (LASCO, Brueckner et al., 1995) on SOHO, and SDO observations to determine the distribution and the emission measure of material along the LoS. Also, persistent observations over at least 2 weeks under identical conditions can be used as rotational “tomography” on long-lived structures.

The Zeeman effect in circular polarization only gives information on the magnetic field projection along the LoS. Thus it provides a lower bound for the true magnetic strength. These measurements are challenging because the circular polarization signal is typically very small in the quiet corona (about 0.1% of the intensity for field strengths of 10 G). Thus a rigorous calibration of all possible sources of polarization noise is fundamental. The extended sequence of observations without atmospheric noise will allow an examination of the ultimate return that can be achieved by these techniques and guide the design and use of future large aperture ground based coronal magnetographs.

Using the saturated Hanlé effect (scattering polarization) applicable in coronal conditions, the PoS direction of the magnetic field can be determined from the linear polarization signal of the scattered radiation, subject in general to a 90° ambiguity (e.g., Lin and Casini, 2000). Where the Stokes

parameters $U = 0$ and $Q \neq 0$, the field coincides with one of axes defined by Q . The ambiguity can be resolved due to the “Van Vleck” effect which causes nulls of linear polarization to occur at a specific angle θ , where $\cos^2\theta = 1/3$, between the magnetic field and the solar vertical. On either side of the null, the polarization direction changes by 90°. Identification of nulls can then be used to tightly constrain the morphology of the magnetic structure. These measurements are much easier, because the linear polarization of the forbidden coronal lines is typically of a few percent. The Fe XIII 1074.7 nm line is chosen because its emission is dominated by scattered disk radiation, and depolarizing effects due to collisions and radiative cascades are insignificant (Judge, 1998). The Fe XIII 1079.8 nm line conversely is dominated by collisions, yielding the density sensitivity of the ratio to the 1074.7 nm line. WAMIS magnetic field observations would additionally be supplemented by the ChroMag full-disk measurements of the chromospheric vector magnetic field, and by measurements of wave propagation in the PoS. Thus the PoS Alfvén speed will be inferred, and with the density from the 1074.7 / 1079.8 nm intensity ratio, or from white light polarization brightness, the PoS magnetic field can also be calculated.

Measurements using both Zeeman effect and Hanlé effect can yield vector field information when the polarized light originates from a defined volume (Casini and Judge, 1999). In those cases constraints can be placed on the inclination of the magnetic field and therefore the total field strength and direction. In cases when a structure possesses substantial uniformity along the LoS (such as polar-crown-filaments and their cavities), magnetic field strength and structure may likewise be determined. **Table 3** lists key observables by WAMIS and the means to obtain them. See **Table 2** for connecting these observables to the science objectives.

WAMIS Instrument Design CoMP as Heritage Instrumentation

The techniques described in Section Coronal Magnetometry via Zeeman and Hanlé Effect have been fully demonstrated with CoMP on the 20 cm aperture OneShot coronagraph originally at National Solar Observatory’s Sacramento Peak Observatory in New Mexico (Tomczyk et al., 2008), and later has been operating on a daily basis at MLSO since 2011. The CoMP instrument was designed to observe the coronal magnetic field with a FOV in the low corona (~ 1.03 to $1.4 R_{\odot}$), as well as to obtain information about the plasma density and motion.

TABLE 3 | Key WAMIS observables.

Line-of-sight B, field strength	Circular polarization	Longitudinal Zeeman effect
Plane-of-sky B, field direction	Linear polarization	Resonance scattering effect (Hanlé effect)
Line of sight velocity	Intensity vs. wavelength	Doppler effect
Plasma density	Fe XIII 1074.7 nm/1079.8 nm intensity ratio, IR continuum	Atomic physics, radiation transfer

The CoMP instrument is a combination polarimeter and narrowband tunable filter that can measure the Doppler shift and complete polarization state of the Fe XIII infrared coronal emission lines at 1074.7 and 1079.8 nm and the chromospheric 1083 nm He I line. The polarimeter function is achieved by a pair of Liquid Crystal Variable Retarders (LCVRs) followed by a linear polarizer that allows the selection of a polarization state characterized by Stokes parameters (I , Q , U , V). The filter is a four-stage, wide-field calcite birefringent filter with a bandwidth of 0.14 nm at 1074.7 nm. It is tuned in wavelength by four additional LCVRs. Both the polarization and filter bandpass selections are accomplished electro-optically. The CoMP filter has a transmission to unpolarized light of about 30%. The camera for CoMP is a liquid nitrogen cooled Rockwell Scientific (now Teledyne) 1024×1024 HgCdTe Infrared detector array. A filter wheel holding three order-blocking filters selects the emission line to be observed. See Tomczyk et al. (2008) for detailed descriptions.

The CoMP observations have a spatial sampling of $4.5''$ per pixel and required 30 min of integration time to acquire a measure of the LoS magnetic field strength. As an example shown in Tomczyk et al. (2008), data were obtained in groups of 60 images in quick succession. For linear polarization, five images were taken at each of the four polarization states I+Q, I−Q, I+U, I−U, and at the three wavelengths, 1074.52, 1074.65, and 1074.78 nm, across the line. For circular polarization, 10 images were taken in each of the two polarization states of I+V and I−V at the same three sample wavelengths. The exposure time for the individual images was 250 ms and the two image groups were each obtained at a cadence of ~ 15 s with a duty cycle of 52%. The driver of the number of image groups (thus integration time) required for a single observation set is the level of sky brightness at MLSO (typically $5 \mu\text{B}_{\odot}$). The WAMIS coronal magnetometer will profit much more from the unique observation conditions obtained at long duration balloon altitudes, because of the absence of sky brightness background as well as seeing-induced polarization cross-talk and atmospheric-induced source intensity fluctuations (Section Advantages of Measurements Outside of the Atmosphere).

WAMIS Filter/Polarimeter

In the time since the completion of the CoMP instrument, technological advances in broad-band polarizers and super-achromatic waveplates now present the possibility to construct a compact coronal polarimeter capable of observing coronal and prominence emission lines over a much wider wavelength range than the CoMP instrument. These advances have been incorporated into a filter/polarimeter called “CoMP-S” built by HAO for the Astronomical Institute of the Slovak Academy of Sciences (AISAS) coronagraph on Lomnický Peak. The CoMP-S filter has been operational on the Lomnický Peak Observatory 20 cm Zeiss coronagraph since April 2013. WAMIS filter will use the same CoMP-S filter/polarimeter design (Kucera et al., 2010; Koza et al., 2013; Rybak et al., 2013).

The CoMP-S design was primarily chosen to enable the WAMIS instrument to observe over the range between the Fe XIV coronal green line at 530.3 nm and the He I line at

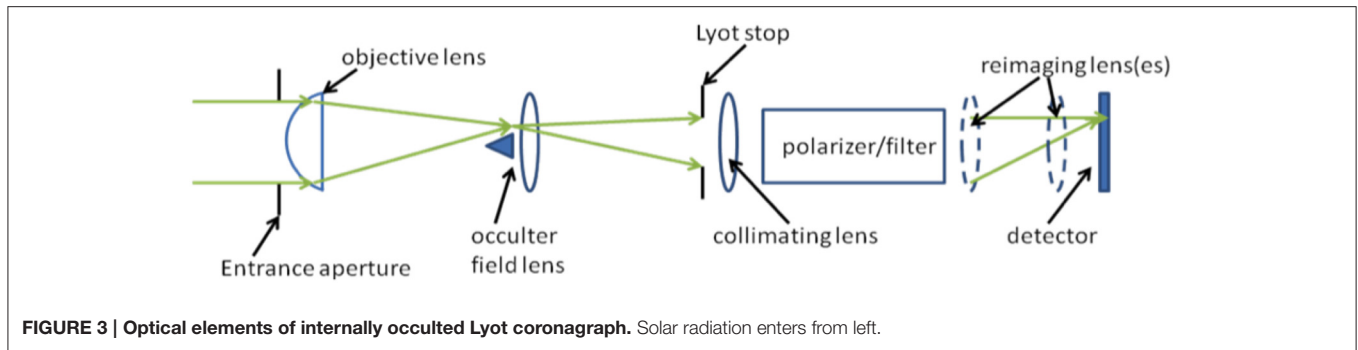
1083 nm. While the target lines for WAMIS are the IR coronal emission lines 1074.7 nm Fe XIII and 1079.8 nm Fe XIII, and the IR prominence emission line 1083.0 nm He I, this filter will have the additional capability to observe corresponding visible lines - including 530.3 nm Fe XIV, 637.5 nm Fe X and 789.2 nm Fe XI in the corona and 587.6 nm He I and 656.3 nm H α in prominences—for context and additional diagnostics. One particularly important diagnostic achieved with this extension of the wavelength range is the capability to observe coronal waves at temperatures other than Fe XIII, e.g., wave observations in coronal hole and coronal hole boundary with Fe X and Fe XI to study the origin of the slow solar wind. Each line will require a pre-filter be inserted in the optical system with a bandpass that depends on the free spectral range of the birefringent filter at that wavelength.

A secondary motivation for using the CoMP-S design is the use of Ferroelectric Liquid Crystals (FLC) in the polarization modulation instead of the usual LCVR. The objective of using FLC is their faster response time, which will significantly increase the duty cycle of the WAMIS instrument. The polarization modulator will consist of two FLC retarders and a fixed retarder followed by a linear polarizer acting as an analyzer. As for CoMP, the polarizer will also act as the entrance polarizer to the birefringent filter. Note that neither the FLCs nor the fixed retarder are achromatic and the value of retardation and orientation must be selected to optimize the Stokes modulation efficiency over a very broad wavelength range.

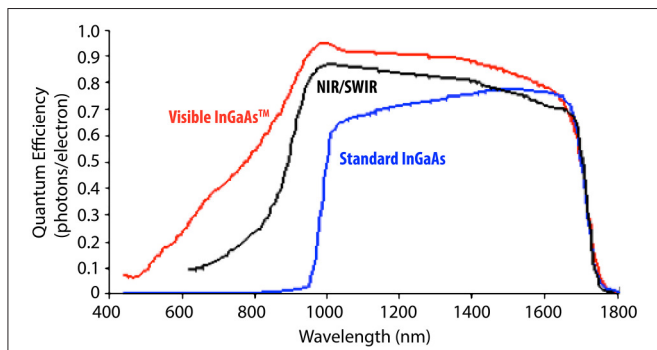
For ground observations, simultaneous images in the emission line and continuum bandpasses is important in that it allows the instrument to be insensitive to variations in the intensity of the background caused by image motion and the passage of atmospheric aerosols through the FOV. For a balloon flight above the atmosphere, no such simultaneous observations are required. However, the K-corona can be sequentially imaged in the continuum at a variety of wavelengths to obtain the electron density information.

WAMIS Coronagraph

The WAMIS coronagraph follows the classic internally occulted Lyot coronagraph design principles (Figure 3). The solar radiation is incident on the entrance aperture. A high quality solar image is produced at the occulter. Coronal radiation from heights of 1.02 to 2.8 R_{\odot} passes through the coronagraph front end and is collimated before entering into the polarizer/filter assembly. A reimaging lens produces a high quality coronal image at the detector. A compensator plate located at the Lyot stop removes spherical aberration in the coronal image at the occulter plane. A polarization calibration optic will be incorporated in front of the instrument aperture to assure the instrumental polarization effects are understood to a level well under 10^{-4} . Table 4 lists the optical design. The resulting plate scale is $4.5''$ for low magnification mode, and $1.5''$ for high magnification mode. The WAMIS coronagraph uses a 20 cm entrance aperture, $f/10$ objective which is sufficient to achieve the scientific requirements in Table 2. The diffraction limit corresponding to this aperture is $1.3''$ at a wavelength of $1 \mu\text{m}$, so diffraction effects are below the plate scale.

**TABLE 4 | Optical design.**

Objective	203.3 cm fl.
Field lens	31.0 cm fl.
Collimating lens	38.0 cm fl.
Re-imaging lens	High Mag. 38.0 cm fl. Low Mag. 12.9 cm fl.

**FIGURE 4 | Detector quantum efficiency (red curve) of the Goodrich Corp. InGaAs High Resolution Visible + SWIR Camera for WAMIS, compared to other camera models (NIR/SWIR and standard InGaAs).**

WAMIS Detector System

WAMIS will use the Goodrich Corp. InGaAs High Resolution Visible+SWIR (short wavelength infrared) Camera as the detector instead of the Teledyne HgCdTe hybrid camera used on CoMP. A single detector for the wide range of wavelength coverage is also beneficial over separate detectors for the visible and IR. The 1280×1024 pixel array focal plane hybrid detector has a 15 micron pitch, achieves 80% quantum efficiency in the target wavelength regime (Figure 4).

Gondola and Pointing Control

There are at least a couple of options to carry instrument under the balloon. An HAO-developed gondola system was successfully used for two Sunrise solar observations in 2009 and 2012 (Barthol et al., 2011). The NASA Wallops Flight Facility (WFF) Balloon

Program Office (BPO) recently has available a gondola system under the Columbia Science Balloon Facility (CSBF), successfully pioneered by the University of Colorado HyperSpectral Imager for Climate Science (HySICS) investigation in 2013. WAMIS high resolution imaging of $1.5''$ requires a matching performance in the pointing control during the balloon flight. The NASA Wallops Arc Second Pointer (WASP) system has achieved a pointing performance of better than $0.25''$ RMS error in both pitch and yaw. This will easily satisfy the WAMIS requirements.

CONCLUDING REMARKS

The fundamental advance of the balloon-borne WAMIS beyond any ground-based coronal magnetograph will come from an effectively complete absence of variability in the polarization background and the extension of the duration of uninterrupted observing by over an order of magnitude. A good analogy for this advancement is the way the SOHO Michelson Doppler Imager (MDI, Scherrer et al., 1995) made fundamental discoveries on photospheric field even though it was preceded by decades of ground based observations by larger instruments. The freedom to explore different temporal regimes without seeing variability or day–night cycle interruptions was the key to these discoveries. Similarly, the fundamental advancements achieved by the near-space observations of WAMIS on coronal magnetic field and waves will point the way for future ground based and orbital instrumentation.

AUTHOR CONTRIBUTIONS

All authors contributed to the science and design of the WAMIS instrument. The first seven authors contributed significantly to the write-up of this manuscript.

ACKNOWLEDGMENTS

This research is supported by the Chief of Naval Research. NCAR is supported by the National Science Foundation.

REFERENCES

- Antiochos, S. K., Mikić, Z., Titov, V. S., Lionello, R., and Linker, J. A. (2011). A model for the sources of the slow solar wind. *Astrophys. J.* 731, 112–122. doi: 10.1088/0004-637X/731/2/112
- Antonucci, E., Gabriel, A. H., and Patchett, B. E. (1984). Oscillations in EUV emission lines during a loop brightening. *Solar Phys.* 93, 85–94.
- Archontis, V. (2008). Magnetic Flux Emergence in the Sun. *J. Geophys. Res.* 113, A03S04. doi: 10.1029/2007ja012422
- Arnaud, J., and Newkirk, G. Jr. (1987). Mean properties of the polarization of the Fe XIII 10747 Å coronal emission line. *Astron. Astrophys.* 178, 263–268.
- Aschwanden, M. J. (1987). Theory of radio pulsations in coronal loops. *Solar Phys.* 111, 113–136. doi: 10.1007/BF00145445
- Aschwanden, M. J., Fletcher, L., Schrijver, C. J., and Alexander, D. (1999). Coronal loop oscillations observed with the transition region and coronal explorer. *Astrophys. J.* 520, 880–894. doi: 10.1086/307502
- Aschwanden, M. J., Winebarger, A., Tsiklauri, D., and Peter, H. (2007). The coronal heating paradox. *Astrophys. J.* 659, 1673–1681. doi: 10.1086/513070
- Asgari-Targhi, M., van Ballegoijen, A. A., Cranmer, S. R., and DeLuca, E. E. (2013). The spatial and temporal dependence of coronal heating by alfvén wave turbulence. *Astrophys. J.* 773, 111–122. doi: 10.1088/0004-637X/773/2/111
- Bak-Steslicka, U., Gibson, S. E., Fan, Y., Bethge, C., Forland, B., and Rachmeler, L. A. (2013). The magnetic structure of solar prominence cavities: new observational signature revealed by coronal magnetometry. *Astrophys. J.* 770, L28–L32. doi: 10.1088/2041-8205/770/2/L28
- Barthol, P., Gandorfer, A., Solanki, S. K., Schüssler, M., Chares, B., Curdt, W., et al. (2011). The Sunrise mission. *Solar Phys.* 268, 1–34. doi: 10.1007/s11207-010-9662-9
- Brooks, D. H., Warren, H. P., Williams, D. R., and Watanabe, T. (2009). Hinode/Extreme ultraviolet imaging spectrometer observations of the temperature structure of the quiet corona. *Astrophys. J.* 705, 1522–1532. doi: 10.1088/0004-637X/705/2/1522
- Brueckner, G. E., Howard, R. A., Koomen, M. J., Korendyke, C. M., Michels, D. J., Moses, J. D., et al. (1995). The Large Angle Spectroscopic Coronagraph (LASCO): visible light coronal imaging and spectroscopy. *Solar Phys.* 162, 357–402. doi: 10.1007/BF00733434
- Bruno, R., and Carbone, V. (2005). The solar wind as a turbulence laboratory. *Living Rev. Solar Phys.* 2:4. doi: 10.12942/lrsp-2005-4
- Casini, R., and Judge, P. G. (1999). Spectral lines for polarization measurements of the coronal magnetic field. II. consistent treatment of the stokes vector for magnetic-dipole transitions. *Astrophys. J.* 522, 524–539. doi: 10.1086/307629
- Chapman, R. D., Jordan, S. D., Neupert, W. M., and Thomas, R. J. (1972). Evidence for the 300-SECOND Oscillation from OSO-7 Extreme-Ultraviolet Observations. *Astrophys. J.* 174, L97–L99. doi: 10.1086/180957
- Ciaravella, A., and Raymond, J. C. (2008). The current sheet associated with the 2003 November 4 coronal mass ejection: density, temperature, thickness, and line width. *Astrophys. J.* 686, 1372–1382. doi: 10.1086/590655
- Ciaravella, A., Raymond, J. C., Li, J., Reiser, P., Gardner, L. D., Ko, Y.-K., et al. (2002). Elemental abundances and post-coronal mass ejection current sheet in a very hot active region. *Astrophys. J.* 575, 1116–1130. doi: 10.1086/341473
- Cirtain, J. W., Golub, L., Lundquist, L., van Ballegoijen, A., Savcheva, A., Shimojo, M., et al. (2007). Evidence for Alfvén Waves in Solar X-ray jets. *Science* 318, 1580–1582. doi: 10.1126/science.1147050
- Cirtain, J. W., Golub, L., Winebarger, A. R., de Pontieu, B., Kobayashi, K., Moore, R. L., et al. (2013). Energy Release in the solar corona from spatially resolved magnetic braids. *Nature* 493, 501–503. doi: 10.1038/nature11772
- De Moortel, I., McIntosh, S. W., Threlfall, J., Bethge, C., and Liu, J. (2014). Potential evidence for the onset of alfvénic turbulence in trans-equatorial coronal loops. *Astrophys. J.* 782, L34–L39. doi: 10.1088/2041-8205/782/2/L34
- De Pontieu, B., Title, A. M., Lemen, J. R., Kushner, G. D., Akin, D. J., Allard, B., et al. (2014). The Interface Region Imaging Spectrograph (IRIS). *Solar Phys.* 289, 2733–2779. doi: 10.1007/s11207-014-0485-y
- De Pontieu, B., McIntosh, S. W., Carlsson, M., Hansteen, V. H., Tarbell, T. D., Schrijver, C. J., et al. (2007). Chromospheric alfvénic waves strong enough to power the solar wind. *Science* 318, 1574–1577. doi: 10.1126/science.1151747
- de Wijn, A. G., Bethge, C., Tomczyk, S., and McIntosh, S. (2012). “The chromosphere and prominence magnetometer,” in *Proceedings of SPIE 8446*, 844678, eds I. S. McLean, S. K. Ramsey, and H. Takami (Amsterdam). doi: 10.1117/12.926395
- Domingo, V., Fleck, B., and Poland, A. I. (1995). The SOHO mission: an overview. *Solar Phys.* 162, 1–37. doi: 10.1007/BF00733425
- Dove, J. B., Gibson, S. E., Rachmeler, L. A., Tomczyk, S., and Judge, P. (2011). A ring of polarized light: evidence for twisted coronal magnetism in cavities. *Astrophys. J.* 731, L1–L5. doi: 10.1088/2041-8205/731/1/L1
- Dulk, G. A., and McLean, D. J. (1978). Coronal magnetic fields. *Solar Phys.* 57, 279–295. doi: 10.1007/BF00160102
- Edmiston, J. P., and Kennel, C. F. (1984). A parametric survey of the first critical mach number for a fast MHD shock. *J. Plasma Phys.* 32, 429–441. doi: 10.1017/S002237780000218X
- Erdélyi, R., and Fedun, V. (2007). Are there alfvén waves in the solar atmosphere? *Science* 318, 1572–1574. doi: 10.1126/science.1153006
- Fan, Y. (2010). On the eruption of coronal flux ropes. *Astrophys. J.* 719, 728–736. doi: 10.1088/0004-637X/719/1/728
- Feldman, U., and Laming, J. M. (2000). Element abundances in the upper atmosphere of the sun and stars: update of observational results. *Phys. Scripta* 61, 222–252. doi: 10.1238/Physica.Regular.061a00222
- Fisk, L. A., and Schwadron, N. A. (2001). Origin of the solar wind: theory. *Space Sci. Rev.* 97, 21–33. doi: 10.1023/A:1011805606787
- Gibson, S. E., Kucera, T. A., Rastawicki, D., Dove, J., de Toma, G., Hao, J., et al. (2010). Three-dimensional morphology of a coronal prominence cavity. *Astrophys. J.* 724, 1133–1146. doi: 10.1088/0004-637X/724/2/1133
- Gopalswamy, N., Lara, A., Kaiser, M. L., and Bougeret, J.-L. (2001). Near-sun and near-earth manifestations of solar eruptions. *J. Geophys. Res.* 106, 25261–25278. doi: 10.1029/2000JA004025
- Hahn, M., Landi, E., and Savin, D. W. (2012). Evidence of wave damping at low heights in a polar coronal hole. *Astrophys. J.* 753, 36–44. doi: 10.1088/0004-637X/753/1/36
- Hahn, M., and Savin, D. W. (2013). Observational quantification of the energy dissipated by alfvén waves in a polar coronal hole: evidence that waves drive the fast solar wind. *Astrophys. J.* 776, 78–87. doi: 10.1088/0004-637X/776/2/78
- Handy, B. N., Acton, L. W., Kankelborg, C. C., Wolfson, C. J., Akin, D. J., Bruner, M. E., et al. (1999). The transition region and coronal explorer. *Solar Phys.* 187, 229–260. doi: 10.1023/A:1005166902804
- Hanslmeier, A. (2003). Space weather - effects of radiation on manned space missions. *Hvar Observatory Bull.* 27, 159–170.
- Harrison, R. A. (1987). Solar soft X-ray pulsations. *Astron. Astrophys.* 182, 337–347.
- Hood, A. W., Archontis, V., Galsgaard, K., and Moreno-Insertis, F. (2009). The emergence of toroidal flux tubes from beneath the solar photosphere. *Astron. Astrophys.* 503, 999–1011. doi: 10.1051/0004-6361/200912189
- House, L. L., Querfeld, C. W., and Rees, D. E. (1982). Coronal emission-line polarization from the statistical equilibrium of magnetic sublevels. II. Fe XIV 5303 Å. *Astrophys. J.* 255, 753–763. doi: 10.1086/159874
- Iucci, N., Dorman, L. I., Levitin, A. E., Belov, A. V., Eroshenko, E. A., Ptitsyna, N. G., et al. (2006). Spacecraft operational anomalies and space weather impact hazards. *Adv. Space Res.* 37, 184–190. doi: 10.1016/j.asr.2005.03.028
- Jess, D. B., Mathioudakis, M., Erdélyi, R., Crockett, P. J., Keenan, F. P., and Christian, D. J. (2009). Alfvén waves in the lower solar atmosphere. *Science* 323, 1582–1585. doi: 10.1126/science.1168680
- Judge, P. G. (1998). Spectral lines for polarization measurements of the coronal magnetic field. I. theoretical intensities. *Astrophys. J.* 500, 1009–1022. doi: 10.1086/305775
- Judge, P. G., Habbal, S., and Landi, E. (2013). From forbidden coronal lines to meaningful coronal magnetic fields. *Solar Phys.* 288, 467–480. doi: 10.1007/s11207-013-0309-5
- Figure, H., Takahashi, K., Shibata, K., Yokoyama, T., and Nozawa, S. (2010). Generation of alfvén waves by magnetic reconnection. *PASJ*, 62, 993–1004. doi: 10.1093/pasj/62.4.993
- Klimchuk, J. A. (2000). Cross-sectional properties of coronal loops. *Solar Phys.* 193, 53–75. doi: 10.1023/A:1005210127703
- Ko, Y.-K., Raymond, J. C., Lin, J., Lawrence, G., Li, J., and Fludra, A. (2003). Dynamical and physical properties of a post-coronal mass ejection current sheet. *Astrophys. J.* 594, 1068–1084. doi: 10.1086/376982
- Koza, J., Ambroz, J., Gomory, P., Habaj, P., Kozak, M., Kucera, A., et al. (2013). “The CoMP-S instrument at the Lomnický Peak Observatory and possible synergy aspects with the space-born observations,” in

- Synergies between Ground and Space Based Solar Research - 1st SOLARNET - 3rd EAST/ATST Meeting* (Oslo). Available online at: http://www.astro.sk/~choc/open/apvv_081611/output/presentations/2013_solarnet_conference_oslo/koza_comp-s_at_LSO_oslo_east_conference.pdf
- Kramar, M., Inhester, B., Lin, H., and Davila, J. (2013). Vector tomography for the coronal magnetic field. II. hanle effect measurements. *Astrophys. J.* 775, 25–36. doi: 10.1088/0004-637X/775/1/25
- Kramar, M., Inhester, B., and Solanki, S. K. (2006). Vector tomography for the coronal magnetic field. I. Longitudinal Zeeman effect measurements. *Astron. Astrophys.* 456, 665–673. doi: 10.1051/0004-6361:20064865
- Krieger, A. S., Timothy, A. F., and Roelof, E. C. (1973). A coronal hole and its identification as the source of a high velocity solar wind stream. *Solar Phys.* 29, 505–525. doi: 10.1007/BF00150828
- Kucera, A., Ambroz, J., Gomory, P., Kozak, M., and Rybak, J. (2010). CoMP-S - the coronal multi-channel polarimeter for Slovakia. *Contrib. Astron. Obs. Skalnaté Pleso.* 40, 135–138.
- Lambour, R. L., Coster, A. J., Clouser, R., Thornton, L. E., Sharma, J., and Cott, T. A. (2003). Operational impacts of space weather. *Geophys. Res. Lett.* 30, 1136. doi: 10.1029/2002gl015168
- Laming, J. M. (2004). A unified picture of the fip and inverse fip effects. *Astrophys. J.* 614, 1063–1072. doi: 10.1086/423780
- Laming, J. M. (2009). Non-WKB models of the FIP effect: implications for solar coronal heating and the coronal helium and neon abundances. *Astrophys. J.* 695, 954–969. doi: 10.1088/0004-637X/695/2/954
- Laming, J. M. (2012). Non-WKB models of the FIP effect: the role of slow mode waves. *Astrophys. J.* 744, 115–127. doi: 10.1088/0004-637X/744/2/115
- Laming, J. M. (2015). The FIP and inverse FIP effects in solar and stellar coronae. *Living Rev. Solar Phys.* 12:2. doi: 10.1007/lrsp-2015-2
- Laming, J. M., Moses, J. D., Ko, Y.-K., Ng, C. K., Rakowski, C. E., and Tylka, A. J. (2013). On the remote detection of suprathermal ions in the solar corona and their role as seeds for solar energetic particle production. *Astrophys. J.* 770, 73–84. doi: 10.1088/0004-637X/770/1/73
- Lin, H., and Casini, R. (2000). A classical theory of coronal emission line polarization. *Astrophys. J.* 542, 528–534. doi: 10.1086/309499
- Lin, H., Kuhn, J. R., and Coulter, R. (2004). Coronal magnetic field measurements. *Astrophys. J.* 613, L177–L180. doi: 10.1086/425217
- Lin, H., Penn, M. J., and Tomczyk, S. (2000). A new precise measurement of the coronal magnetic field strength. *Astrophys. J.* 541, L83–L86. doi: 10.1086/312900
- Liu, J., McIntosh, S. W., De Moortel, I., Threlfall, J., and Bethge, C. (2014). Statistical evidence for the existence of alfvénic turbulence in solar coronal loops. *Astrophys. J.* 797, 7–16. doi: 10.1088/0004-637X/797/1/7
- Liu, Y.-H., Drake, J. F., and Swisdak, M. (2011). The effects of strong temperature anisotropy on the kinetic structure of collisionless slow shocks and reconnection exhausts. part I. particle-in-cell simulations. *Phys. Plasmas* 18, 062110. doi: 10.1063/1.3627147
- Longcope, D. W., Guidoni, S. E., and Linton, M. G. (2009). Gas-Dynamic shock heating of post-flare loops due to retraction following localized impulsive reconnection. *Astrophys. J.* 690, L18–L22. doi: 10.1088/0004-637X/690/1/L18
- Lynch, B. J., Antiochos, S. K., MacNeice, P. J., Zurbuchen, T. H., and Fisk, L. A. (2004). Observable properties of the breakout model for coronal mass ejections. *Astrophys. J.* 617, 589–599. doi: 10.1086/424564
- Malanushenko, A., and Schrijver, C. J. (2013). On anisotropy in expansion of magnetic flux tubes in the solar corona. *Astrophys. J.* 775, 120–135. doi: 10.1088/0004-637X/775/2/120
- Mann, G., Klassen, A., Aurass, H., and Classen, H.-T. (2003). Formation and development of shock waves in the solar corona and the near-sun interplanetary space. *Astron. Astrophys.* 400, 329–336. doi: 10.1051/0004-6361:20021593
- McIntosh, S. W., and De Pontieu, B. (2012). Estimating the “Dark” energy content of the solar corona. *Astrophys. J.* 761, 138–145. doi: 10.1088/0004-637X/761/2/138
- McIntosh, S. W., De Pontieu, B., Carlsson, M., Hansteen, V., Boerner, P., and Goossens, M. (2011). Alfvénic waves with sufficient energy to power the quiet solar corona and fast solar wind. *Nature* 475, 477–480. doi: 10.1038/nature10235
- Morton, R. J., Tomczyk, S., and Pinto, R. (2015). Investigating alfvénic wave propagation in coronal open-field regions. *Nat. Commun.* 6, 7813. doi: 10.1038/ncomms8813
- Nakariakov, V. M., Ofman, L., DeLuca, E. E., Roberts, B., and Davila, J. M. (1999). TRACE observation of damped coronal loop oscillations: implications for coronal heating. *Science* 285, 862–864. doi: 10.1126/science.285.54.29.862
- Ng, C. K., and Reames, D. V. (2008). Shock acceleration of solar energetic protons: the first ten minutes. *Astrophys. J.* 686, L123–L126. doi: 10.1086/592996
- Okamoto, T. J., and De Pontieu, B. (2011). Propagating waves along spicules. *Astrophys. J.* 736, L24–L29. doi: 10.1088/2041-8205/736/2/L24
- Orozco Suárez, D., Asensio Ramos, A., and Trujillo Bueno, J. (2014). The magnetic field configuration of a solar prominence inferred from spectropolarimetric observations in the He I 10830 Å triplet. *Astron. Astrophys.* 566, A46. doi: 10.1051/0004-6361/201322903
- Patsourakos, S., Vourlidas, A., and Stenborg, G. (2013). Direct evidence for a fast coronal mass ejection driven by the prior formation and subsequent destabilization of a magnetic flux rope. *Astrophys. J.* 764, 125–137. doi: 10.1088/0004-637X/764/2/125
- Penn, M. J., H., Lin, S., Tomczyk, D., and Elmore, P., (Judge) (2004). Background-induced measurement errors of the coronal intensity, density, velocity and magnetic field. *Solar Phys.* 222, 61–78. doi: 10.1023/B:SOLA.0000036850.34404.5f
- Pesnell, W. D., Thompson, B. J., and Chamberlain, P. C. (2012). The Solar Dynamics Observatory (SDO). *Solar Phys.* 275, 3–15. doi: 10.1007/s11207-011-9841-3
- Peter, H. (2001). On the nature of the transition region from the chromosphere to the corona of the sun. *Astron. Astrophys.* 374, 1108–1120. doi: 10.1051/0004-6361:20010697
- Peter, H. (2010). Asymmetries of solar coronal extreme ultraviolet emission lines. *Astron. Astrophys.* 521, A51. doi: 10.1051/0004-6361/201014433
- Peter, H., Bingert, S., Klimchuk, J. A., de Forest, C., Cirtain, J. W., Golub, L., et al. (2013). Structure of solar coronal loops: from miniature to large-scale. *Astron. Astrophys.* 556, A104. doi: 10.1051/0004-6361/201321826
- Rachmeler, L. A., Gibson, S. E., Dove, J. B., DeVore, C. R., and Fan, Y. (2013). Polarimetric properties of flux ropes and sheared arcades in coronal prominence cavities. *Solar Phys.* 288, 617–636. doi: 10.1007/s11207-013-0325-5
- Rachmeler, L. A., Platten, S. J., Bethge, C., Seaton, D. B., and Yeates, A. R. (2014). Observations of a hybrid double-streamer/pseudostreamer in the solar corona. *Astrophys. J.* 787, L3–L8. doi: 10.1088/2041-8205/787/1/L3
- Rakowski, C. E., and Laming, J. M. (2012). On the origin of the slow speed solar wind: helium abundance variations. *Astrophys. J.* 754, 65–74. doi: 10.1088/0004-637X/754/1/65
- Régnier, S. (2013). Magnetic field extrapolations in the corona: success and future improvements. *Solar Phys.* 288, 481–505. doi: 10.1007/s11207-013-0367-8
- Roberts, B., Edwin, P. M., and Benz, A. O. (1983). Fast pulsations in the solar corona. *Nature* 305, 688–690. doi: 10.1038/305688a0
- Rouillard, A. P., Odstřil, D., Sheeley, N. R., Tylka, A., Vourlidas, A., Mason, G., et al. (2011). Interpreting the properties of solar energetic particle events by using combined imaging and modeling of interplanetary shocks. *ApJ*, 735, 7–17. doi: 10.1088/0004-637X/735/1/7
- Rybak, J., Ambroz, J., Gomory, P., Habaj, P., Koza, J., Kozak, M., et al. (2013). *Coronal Multi-channel Polarimeter at the Lomnický Peak Observatory: CoMP-S@LSO, Kanzelhohe Colloquium*, (Treffen), Austria. Available online at: http://www.astro.sk/~choc/open/apvv_0816-11/output/presentations/2013_kanzelhohe_colloquium_2013/rybak_comp-s_at_los_kso70.pdf
- Sakai, J. I., Minamizuka, R., Kawata, T., and Cramer, N. F. (2001). Nonlinear torsional and compressional waves in a magnetic flux tube with electric current near the quiet solar photospheric network. *Astrophys. J.* 550, 1075–1092. doi: 10.1086/319802
- Savage, S. L., McKenzie, D. E., Reeves, K. K., Forbes, T. G., and Longcope, D. W. (2010). Reconnection outflows and current sheet observed with Hinode/XRT in the 2008 April 9 “Cartwheel CME” Flare. *Astrophys. J.* 722, 329–342. doi: 10.1088/0004-637X/722/1/329
- Scherrer, P. H., Bogart, R. S., Bush, R. I., Hoeksema, J. T., Kosovichev, A. G., Schou, J., et al. (1995). The solar oscillations investigation–michelson doppler imager. *Sol. Phys.* 162, 129–188. doi: 10.1007/BF00733429
- Schrijver, C. J., Title, A. M., Berger, T. E., Fletcher, L., Hurlburt, N. E., Nightingale, R. W., et al. (1999). A new view of the solar outer atmosphere by the transition region and coronal explorer. *Sol. Phys.* 187, 261–302. doi: 10.1023/A:1005194519642

- Sturrock, P. A. (1999). Chromospheric magnetic reconnection and its possible relationship to coronal heating. *Astrophys. J.* 521, 451–459. doi: 10.1086/307544
- Testa, P., De Pontieu, B., Martínez-Sykora, J., DeLuca, E., Hansteen, V., Cirtain, J., et al. (2013). Observing coronal nanoflares in active region moss. *Astrophys. J.* 770, L1–L7. doi: 10.1088/2041-8205/770/1/L1
- Thurgood, J. O., and McLaughlin, J. A. (2013). 3D Alfvén wave behaviour around proper and improper magnetic null points. *Astron. Astrophys.* 558, A127. doi: 10.1051/0004-6361/201322021
- Tian, H., Tomczyk, S., McIntosh, S. W., Bethge, C., de Toma, G., and Gibson, S. (2013). Observations of coronal mass ejections with the coronal multichannel polarimeter. *Solar Phys.* 288, 637–650. doi: 10.1007/s11207-013-0317-5
- Tomczyk, S., Card, G. L., Darnell, T., Elmore, D. F., Lull, R., Nelson, P. G., et al. (2008). An instrument to measure coronal emission line polarization. *Solar Phys.* 247, 411–428. doi: 10.1007/s11207-007-9103-6
- Tomczyk, S., and McIntosh, S. W. (2009). Time-distance seismology of the solar corona with CoMP. *Astrophys. J.* 697, 1384–1391. doi: 10.1088/0004-637X/697/2/1384
- Tomczyk, S., McIntosh, S. W., Keil, S. L., Judge, P. G., Schad, T., Seeley, D. H., et al. (2007). Alfvén waves in the solar corona. *Science* 317, 1192–1196. doi: 10.1126/science.1143304
- Tylka, A. J., and Lee, M. A. (2006). A model for spectral and compositional variability at high energies in large, gradual solar particle events. *Astrophys. J.* 646, 1319–1334. doi: 10.1086/505106
- Ugarte-Urra, I., Warren, H. P., and Wineberger, A. R. (2007). The magnetic topology of coronal mass ejection sources. *Astrophys. J.* 662, 1293–1301. doi: 10.1086/514814
- Van Doorselaere, T., Nakariakov, V. M., and Verwichte, E. (2008). Detection of waves in the solar corona: kink or alfvén? *Astrophys. J.* 676, L73–L75. doi: 10.1086/587029
- Vasheghani Farahani, S., Nakariakov, V. M., and Doorselaere, T. (2010). Long wavelength torsional modes of solar coronal plasma structures. *Astron. Astrophys.* 517, A29. doi: 10.1051/0004-6361/201014502
- von Steiger, R., Wimmer Schweingruber, R. F., Geiss, J., and Gloeckler, G. (1995). Abundance variations in the solar wind. *Adv. Space Res.* 15, 3–12. doi: 10.1016/0273-1177(94)00013-Q
- Vourlidas, A., Wu, S. T., Wang, A. H., Subramanian, P., and Howard, R. A. (2003). Direct detection of a coronal mass ejection-associated shock in large angle and spectrometric coronagraph experiment white-light images. *Astrophys. J.* 598, 1392–1402. doi: 10.1086/379098
- Wang, T. J., Ofman, L., and Davila, J. M. (2009). Propagating slow magnetoacoustic waves in coronal loops observed by hinode/EIS. *Astrophys. J.* 696, 1448–1460. doi: 10.1088/0004-637X/696/2/1448
- Warren, H. P., Winebarger, A. R., and Brooks, D. H. (2010). Evidence for steady heating: observations of an active region core with Hinode and TRACE. *Astrophys. J.* 711, 228–238. doi: 10.1088/0004-637X/711/1/228
- Wiegmann, T., and Sakurai, T. (2012). Solar force-free magnetic fields. *Living Rev. Solar Phys.* 9:5. doi: 10.12942/lrsp-2012-5

Conflict of Interest Statement: The authors declare that the research was conducted in the absence of any commercial or financial relationships that could be construed as a potential conflict of interest.

Copyright © 2016 Ko, Moses, Laming, Strachan, Tun Beltran, Tomczyk, Gibson, Auchère, Casini, Fineschi, Knoelker, Korendyke, McIntosh, Romoli, Rybak, Socker, Vourlidas and Wu. This is an open-access article distributed under the terms of the Creative Commons Attribution License (CC BY). The use, distribution or reproduction in other forums is permitted, provided the original author(s) or licensor are credited and that the original publication in this journal is cited, in accordance with accepted academic practice. No use, distribution or reproduction is permitted which does not comply with these terms.